

The Molecule-Metal Bond of Alternant versus Nonalternant Aromatic Systems on Coinage Metal Surfaces: Naphthalene versus Azulene on Ag(111) and Cu(111)

Benedikt P. Klein, Juliana M. Morbec, Markus Franke, Katharina K. Greulich, Malte Sachs, Shayan Parhizkar, François C. Bocquet, Martin Schmid, Samuel J. Hall, Reinhard J. Maurer, Bernd Meyer, Ralf Tonner, Christian Kumpf, Peter Kratzer, and J. Michael Gottfried

J. Phys. Chem. C, **Just Accepted Manuscript** • DOI: 10.1021/acs.jpcc.9b08824 • Publication Date (Web): 06 Nov 2019

Downloaded from pubs.acs.org on November 8, 2019

Just Accepted

“Just Accepted” manuscripts have been peer-reviewed and accepted for publication. They are posted online prior to technical editing, formatting for publication and author proofing. The American Chemical Society provides “Just Accepted” as a service to the research community to expedite the dissemination of scientific material as soon as possible after acceptance. “Just Accepted” manuscripts appear in full in PDF format accompanied by an HTML abstract. “Just Accepted” manuscripts have been fully peer reviewed, but should not be considered the official version of record. They are citable by the Digital Object Identifier (DOI®). “Just Accepted” is an optional service offered to authors. Therefore, the “Just Accepted” Web site may not include all articles that will be published in the journal. After a manuscript is technically edited and formatted, it will be removed from the “Just Accepted” Web site and published as an ASAP article. Note that technical editing may introduce minor changes to the manuscript text and/or graphics which could affect content, and all legal disclaimers and ethical guidelines that apply to the journal pertain. ACS cannot be held responsible for errors or consequences arising from the use of information contained in these “Just Accepted” manuscripts.

1
2
3 **The Molecule-Metal Bond of Alternant versus Nonalternant Aromatic**
4 **Systems on Coinage Metal Surfaces: Naphthalene versus Azulene on**
5 **Ag(111) and Cu(111)**
6
7
8
9
10
11
12

13 Benedikt P. Klein^a, Juliana M. Morbec^b, Markus Franke^c, Katharina K. Greulich^a,
14 Malte Sachs^a, Shayan Parhizkar^c, François C. Bocquet^c, Martin Schmid^a,
15 Samuel J. Hall^{d,e}, Reinhard J. Maurer^c, Bernd Meyer^f, Ralf Tonner^a,
16 Christian Kumpf^c, Peter Kratzer^b, J. Michael Gottfried^{a*}
17
18
19
20

21 ^a*Fachbereich Chemie, Philipps-Universität Marburg, Hans-Meerwein-Straße 4, 35032*
22 *Marburg, Germany*
23

24 ^b*Fakultät für Physik, Universität Duisburg-Essen, Lotharstraße 1, 47048 Duisburg,*
25 *Germany*
26
27

28 ^c*Peter Grünberg Institut (PGI-3), Forschungszentrum Jülich, 52425 Jülich, Germany and*
29 *Jülich Aachen Research Alliance (JARA) – Fundamentals of Future Information*
30 *Technology, 52425 Jülich, Germany*
31

32 ^d*MAS Centre for Doctoral Training, Senate House, University of Warwick, Gibbet Hill*
33 *Road, Coventry, CV4 7AL, United Kingdom*
34
35

36 ^e*Department of Chemistry and Centre for Scientific Computing, University of Warwick,*
37 *Gibbet Hill Road, Coventry, CV4 7AL, United Kingdom*
38

39 ^f*Interdisciplinary Center for Molecular Materials (ICMM) and Computer-Chemistry-*
40 *Center (CCC), Friedrich-Alexander-Universität Erlangen-Nürnberg, Nögelsbachstraße*
41 *25, 91052 Erlangen, Germany*
42
43
44
45
46
47
48
49
50
51
52
53
54
55
56
57
58
59
60

ABSTRACT

Interfaces between polycyclic π -electron systems and metals play prominent roles in organic or graphene-based (opto)electronic devices, in which performance-related parameters depend critically on the properties of metal/semiconductor contacts. Here, we explore how the topology of the π -electron system influences the bonding and the electronic properties of the interface. We use azulene as a model for nonalternant pentagon-heptagon (5-7) ring pairs and compare it to its isomer naphthalene, which represents the alternant 6-6 ring pair. Their coverage-dependent interaction with Ag(111) and Cu(111) surfaces was studied with the normal-incidence X-ray standing wave (NIXSW) technique, near-edge X-ray absorption fine structure (NEXAFS) spectroscopy, UV and X-ray photoelectron spectroscopy (UPS, XPS), and density functional theory (DFT). Coverage-dependent adsorption heights and spectroscopic data reveal that azulene forms shorter interfacial bonds than naphthalene and engages in stronger electronic interactions with both surfaces. These differences are more pronounced on Cu. Increasing coverages lead to larger adsorption heights, indicating bond weakening by intermolecular repulsion. The extensive DFT calculations include dispersive interactions using: (1) the DFT-D3 scheme, (2) the vdW^{surf} correction based on DFT-TS, (3) a Many-Body Dispersion (MBD) correction scheme, and (4) the D3^{surf} scheme. All methods predict the adsorption heights reasonably well with an average error below 0.1 Å. The stronger bond of azulene is attributed to its nonalternant topology, which results in a reduced HOMO-LUMO gap and brings the LUMO energetically close to the Fermi energy of the metal, causing stronger hybridization with electronic states of the metal surfaces.

INTRODUCTION

Semiconductor materials with polycyclic π -electron systems such as aromatic molecules,¹ polymers,² and graphene derivatives³ are widely applied in organic (opto)electronic devices such as organic light-emitting diode (OLED) based displays,⁴⁻⁵ where the semiconductors are typically contacted by metal electrodes.⁶⁻¹⁰ The resulting metal/organic interfaces determine important performance-related parameters such as charge carrier injection rates¹¹ and have therefore been in the focus of surface-science studies with various model systems.¹²⁻¹⁸ The molecules used in these studies, such as benzene,¹⁸ pentacene,¹⁴⁻¹⁵ 3,4,9,10-perylene tetracarboxylic dianhydride (PTCDA),¹⁶ or sexiphenyl (6T),¹⁷ often comprise aromatic carbon backbones with alternant topologies. The latter term is rooted in the Hückel molecular orbital (HMO) theory, in which the linking pattern between the atoms in the conjugated system is expressed by the topological matrix and can be alternant or nonalternant.¹⁹ An alternant topology means that the atoms of two mutually exclusive subsets (*e.g.* red and green labelled atoms in Figure 1) are linked such that only atoms of different sets form direct bonds. Typical alternant aromatic hydrocarbons, such as naphthalene, consist of hexagonal rings (Figure 1a). In contrast, nonalternant structures contain bonds between atoms of the same subset. A prototypical example is azulene (Figure 1b), an isomer of naphthalene, with its pentagon-heptagon (5-7) ring-pair structure. Comparison of the two isomers reveals the large influence of the topology on the optical and electronic properties: Azulene has a blue color and a considerable dipole moment of 0.8 D,²⁰ while the non-polar naphthalene does not absorb in the visible range.

Because of their unique properties, molecules with nonalternant aromatic backbones have found increasing interest for application in organic (opto)electronic devices.²¹ Nonalternant structures also occur as defects in graphene, especially the 5-7 ring-pair motif of azulene. Such defects in graphene are potentially important because of the reduced contact resistance at defect sites.⁹ Despite their relevance for the understanding of metal/semiconductor and metal/graphene contacts, interfaces of nonalternant aromatic structures have rarely been investigated and compared to the corresponding alternant structures. Only very recently, it has been shown that azulene engages in a stronger bond to a Cu(111) surface than naphthalene.²²

Here, we present an extended investigation of metal/organic interfaces of alternant versus nonalternant molecules. Expanding on previous work,²² we compare the interaction of azulene and naphthalene with Ag(111) and Cu(111) surfaces at different coverages. For the first time, we present coverage-dependent adsorption heights, as measured by the NIXSW technique, and work-function changes for these systems, along with extensive theoretical treatment. Photoemission and NEXAFS data in combination with DFT calculations reveal details of the surface chemical bond in all systems. The theory part is of unprecedented depth for this class of systems: we compare four different methods for the prediction of the critical van der Waals contribution to the surface chemical bond: (1) the DFT-D3 scheme with Becke-Johnson damping function,²³⁻²⁴ (2) the vdW^{surf} correction²⁵ based on DFT-TS,²⁶⁻²⁸ (3) a Many-Body Dispersion (MBD) correction scheme,²⁹⁻³⁰ and (4) the D3^{surf} scheme (see the Supporting Information (SI) for details).

Our results reveal substantial influences of the topology on the interfacial chemical bond. The detailed experimental and theoretical investigation clarifies the mechanisms behind the different modes of interaction and thereby also contributes to the understanding of real metal-graphene contacts.

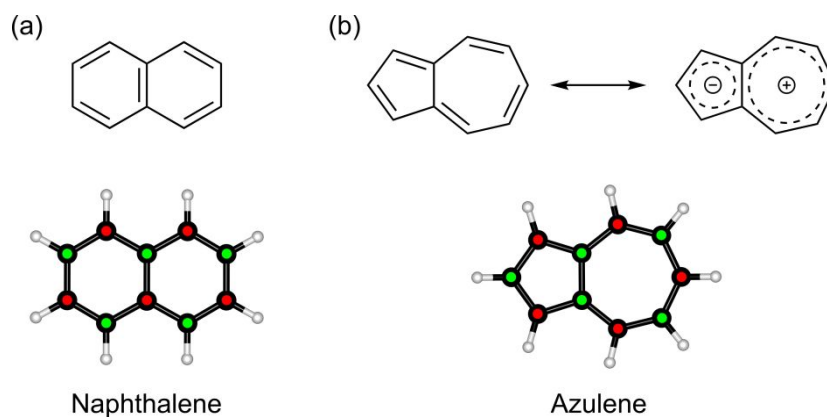


Figure 1. Molecular structures of (a) naphthalene and (b) azulene. The dipolar nature of azulene is illustrated by the additional mesomeric structure (right). The different topologies of the two isomers are illustrated by the schemes in the bottom row: naphthalene has an alternant topology (direct bonds only between differently labelled centers), whereas azulene has a nonalternant topology (direct bond between two atoms with the same color label).

METHODS

A. Experimental Methods

The interaction of azulene and naphthalene with Cu(111) and Ag(111) was studied under ultrahigh-vacuum (UHV) conditions. Azulene (Sigma-Aldrich, purity >99.0 %) and naphthalene (Sigma-Aldrich, purity >99.7 %) were introduced into the vacuum systems through leak valves after initial pump-freeze-thaw cycles of the stainless-steel reservoirs. The polished single-crystal surfaces (purity >99.9999 % for Cu(111) and >99.999 % for Ag(111), roughness < 0.01 μm , orientation accuracy < 0.1°, from MaTeck/Germany) were prepared by iterated sputtering with Ar^+ ions (0.5-1 keV, 5-15 μA , 30 min) and annealing (800-830 K, 15 min). Surface cleanliness and structure were confirmed by XPS, low energy electron diffraction (LEED) and scanning tunneling microscopy (STM). Sample temperatures were measured with type K thermocouples directly mounted to the single crystals. Coverages are given in monolayers (ML), where a coverage of 1 ML represents a complete layer of the molecule on the surface. The absolute monolayer coverage was determined as described previously²² and amounts to 0.16 molecules per surface atom on the Ag(111) surface and 0.13 molecules per surface atom on the Cu(111) surface.

X-ray photoelectron spectroscopy (XPS) and normal incidence X-ray standing wave (NIXSW) measurements were performed at the undulator beamline I-09 at Diamond Light Source in Didcot, UK. For photoelectron detection, a VG Scienta EW4000 HAXPES

1
2
3 hemispherical electron analyzer mounted at 90° with respect to the incident X-ray beam
4 was used. The data analysis was performed using the software package TORRICELLI,³¹⁻³²
5 including the correction of non-dipolar effects.³³ The sample temperature was
6 approximately 150 K, which leads to Bragg energies of 2980 and 2638 eV for the (111)
7 lattices planes of Cu and Ag, respectively. The photon energy for the XPS measurements
8 was 600 eV.
9

10
11
12 UV photoelectron spectroscopy (UPS) was performed with He-I and He-II radiation from
13 a UVS 10/35 gas discharge lamp and a PHOIBOS 150 electron energy analyzer equipped
14 with an MCD-9 multi channeltron detector. Work functions were measured with the same
15 setup.
16

17
18 Near-edge X-ray absorption fine structure (NEXAFS) spectroscopy was performed at the
19 synchrotron radiation facility BESSY II (Helmholtz-Zentrum Berlin) using the HE-SGM
20 dipole beamline, which provides linearly polarized radiation with a polarization factor of
21 0.91 and an energy resolution of 300 meV at the carbon K-edge. The partial electron-yield
22 (PEY) mode was used with a retarding field of -150 V and a channeltron detector voltage
23 of 2.2 keV. The resulting NEXAFS data was treated as described previously.²²
24
25

26 27 28 **B. Density Functional Theory Calculations**

29
30 Density-functional-theory calculations using periodic boundary conditions were performed
31 to compute adsorption heights and work-function changes. The generalized gradient
32 approximation (GGA) proposed by Perdew, Burke, and Ernzerhof (PBE)³⁴ for the
33 exchange-correlation functional was used in combination with four different methods to
34 treat the van der Waals (vdW) interactions: (1) the DFT-D3 scheme with Becke-Johnson
35 damping function,²³⁻²⁴ (2) the vdW^{surf} correction²⁵ based on DFT-TS,²⁶⁻²⁸ (3) a Many-Body
36 Dispersion (MBD) correction scheme,²⁹⁻³⁰ and (4) the D3^{surf} scheme. Below, a brief
37 description of the computational methods is given. Further details can be found in the SI.
38
39

40
41
42 The DFT-D3 scheme proposed by Grimme *et al.* uses atomic pairwise contributions to the
43 dispersion interaction energy based on the polarization of the respective atoms in their
44 chemical environment.³⁵ The energy contributions are based on tabulated C_6 coefficients
45 taking into account the fractional coordination number of the atom under consideration and
46 a damping function for close interatomic distances following a proposal by Becke and
47 Johnson.²³⁻²⁴
48

49
50
51 The vdW^{surf} approach²⁵ includes the collective electronic response of the substrate in the
52 determination of the vdW parameters (C_6 coefficients, polarizabilities and vdW radii) by
53 combining the pairwise Tkatchenko-Scheffler (TS) method²⁶ with the Lifshitz-Zaremba-
54 Kohn theory.²⁷⁻²⁸
55

56
57 The MBD method²⁹⁻³⁰ accounts for collective vdW effects beyond the pairwise
58 approximation by including self-consistent screening of the atomic TS polarizabilities. This
59 is achieved by representing the atomic response functions (within the random phase
60

approximation) by a set of quantum harmonic oscillators interacting via a coupled fluctuating dipole model.

The D3^{surf} scheme is an extension of the original DFT-D3 method proposed by Grimme *et al.* in which the parameter set of coordination-dependent C₆ coefficients is extended by additional values for Cu and Ag at the higher coordination numbers of the surface and bulk atoms, as explained in detail in the SI.

X-ray absorption spectra were calculated using the pseudopotential plane-wave code CASTEP-17.1³⁶. For the XPS chemical shifts the delta self-consistent field (DeltaSCF) method of constraining electronic occupations to resemble full core-hole excitations was used. NEXAFS calculations were performed using on-the-fly generated USPPs in the CASTEP module ELNES³⁷ and the transition-potential approach.³⁸⁻³⁹ For more details on the computational settings and analysis see the SI and Diller *et al.*⁴⁰ For more details on the implementation of the molecular orbital projection employed in Figure 9, see Maurer and Reuter.⁴¹

RESULTS

Adsorbate-substrate bond distances (Adsorption heights)

The height of an adsorbed molecule above the surface, *i.e.*, its vertical bonding distance, is an important criterion for determining the character of a surface chemical bond. A unique method to measure adsorption heights is the normal incidence X-ray standing wave (NIXSW) technique. As this method is described elsewhere in detail,⁴²⁻⁴⁴ we only give a short description here. When monochromatic X-rays undergo Bragg reflection on a crystalline substrate, a standing wave field is formed. Variation of the photon energy around the Bragg condition leads to a phase shift and thus changes the position of the nodes and anti-nodes of the standing wave field relative to the crystal planes. Therefore, the X-ray intensity at any given height has a characteristic energy-dependent profile. Any quantity that is proportional to the photon intensity, such as the photoelectron intensity in a photoemission experiment, follows the same profile. This profile (yield profile) can be extracted for each XPS signal and be analyzed with a fit-model derived by dynamical diffraction theory including the corrections of non-dipolar effects:^{31, 33, 42-44}

$$I(E) = 1 + S_R R + 2|S_I| \sqrt{R} \cdot F^H \cdot \cos(\Phi - 2\pi P^H + \Psi) \quad (1)$$

Here, $I(E)$ is the (photon)energy-dependent XPS intensity, $R = R(E)$ is the reflectivity (intensity of the Bragg reflection H), and $\Phi = \Phi(E)$ is the phase of the standing wave field. S_R , $|S_I|$ and Ψ are correction parameters to the yield model taking into account the dipole-quadrupole approximation of the photoemission process (the so-called non-dipolar effect, see the literature³³ and the SI for details).

The fitting procedure yields the coherent position P^H and the coherent fraction F^H . P^H represents the height relative to the next lattice planes below, in units of the lattice spacing d_H , while F^H is a measure for the vertical order. Typically, $F^H = 1$ indicates that all related

atoms have the same adsorption height (as expressed by P^H), whereas $F^H = 0$ means randomly distributed heights.

Using this method, we determined the adsorption heights of azulene and naphthalene on Cu(111) and Ag(111) at various coverages. The values of P^H and F^H for all measurements are compiled (in Table S1) and visualized in Argand vector diagrams (in Figure S1) in the SI. From the coherent positions, the monolayer adsorption heights D^H were extracted using $D^H = (P^H + n) d_H$, where n is the number of lattice planes that would fit between the sample surface and the adsorbate layer. At monolayer coverage (1 ML), the adsorption heights for azulene are $2.30(\pm 0.03)$ Å on Cu(111) and $3.06(\pm 0.02)$ Å on Ag(111). For naphthalene, the corresponding values are $3.03(\pm 0.04)$ Å on Cu(111) and $3.13(\pm 0.02)$ Å on Ag(111) (Figure 2a). On Ag(111), both distances are in line with previously reported values for cases of physisorption of planar organic molecules on Ag.^{18, 45} There is no indication from other methods pointing to a covalent chemical bond, although both molecules are slightly closer to the surface than the sum of their tabulated van-der-Waals radii (3.42 Å).⁴⁶ In the case of the Cu(111) surface, the adsorption height of naphthalene is close to the sum of the van-der-Waals radii (3.1 Å).⁴⁶ In contrast, the height of azulene approaches that of a typical carbon-copper bond length (2.2 Å),²⁰ indicating a strong chemical interaction in this system, which is supported by a variety of other experimental and theoretical methods.

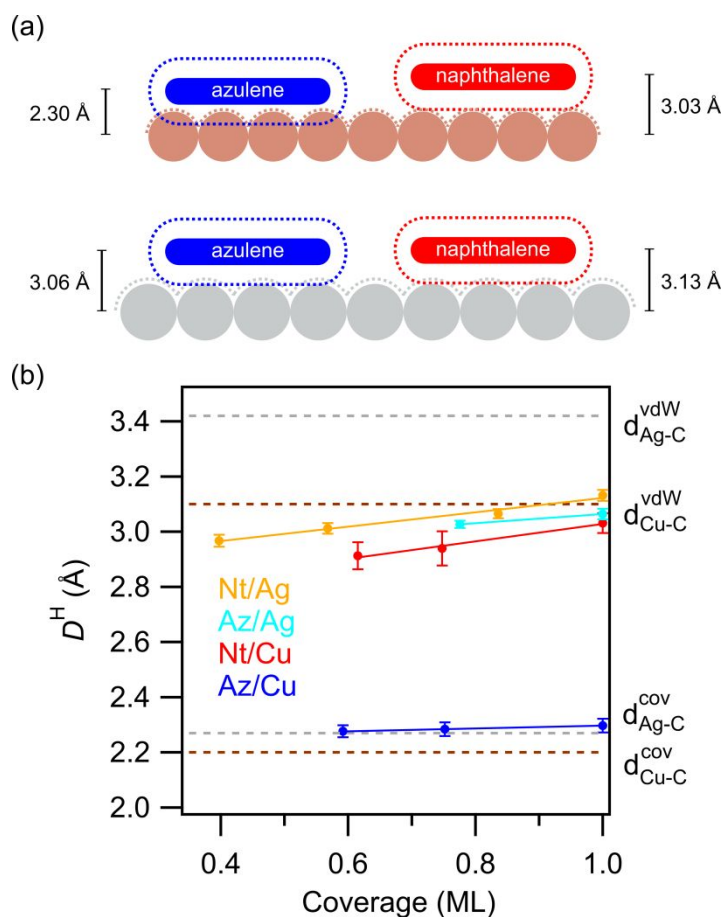


Figure 2. (a) NIXSW adsorption heights of azulene (Az) and naphthalene (Nt) at monolayer coverage. The filled areas represent the covalent radii,²⁰ while the dashed lines represent the vdW radii.⁴⁶ (b) Coverage-dependent adsorption heights for all four systems,

based on the NIXSW data in Table 1. The uncertainty in the coverage is in the range of 0.05 ML. The horizontal dashed lines indicate the corresponding vdW and covalent distances calculated from literature vdW⁴⁶ and covalent²⁰ radii.

The results of the NIXSW measurements at various coverages are summarized in Table 1 and Figure 2b. The coverages were determined from the XPS intensities. The NIXSW results show a slight increase of adsorption height with the coverage for all systems, which is to be expected and in agreement with the coverage dependence of the adsorption energy known for these and other systems.^{45, 47-49} Commonly, this is attributed to the lateral repulsion between the molecules and subsequent weakening of the bond with increasing coverage.^{48, 50}

The values of the coherent fraction F^H are all in a reasonable range for organic molecules of this size,^{18, 51} if corrections for non-dipolar effects are included.³³ The Argand diagrams for all NIXSW measurements from Table 1 and a comparison showing the influence of the non-dipolar effects on the analysis are provided in the SI.

Table 1. Coverage dependent results of the NIXSW measurements. All coverages Θ are in ML, all adsorption heights D^H are in Å. The uncertainty in the coverages is about 0.05 ML.

Molecule	Surface	Θ D^H	Θ D^H	Θ D^H	Θ D^H
Azulene	Cu(111)		0.59 2.28 (±0.02)	0.75 2.28 (±0.02)	1.0 2.30 (±0.03)
	Ag(111)			0.78 3.03 (±0.01)	1.0 3.06 (±0.02)
Naphthalene	Cu(111)		0.59 2.91 (±0.05)	0.75 2.94 (±0.06)	1.0 3.03 (±0.04)
	Ag(111)	0.40 2.97 (±0.02)	0.57 3.01 (±0.02)	0.84 3.07 (±0.02)	1.0 3.13 (±0.02)

Occupied electronic states: Photoelectron spectroscopy

The occupied electronic states, which are expected to reflect properties of the interfacial chemical bond, were probed here with X-ray and UV photoelectron spectroscopy. The core level C 1s spectra for monolayers of both molecules adsorbed on Cu(111) and Ag(111) are shown in Figure 3a. As can be seen, the signals of naphthalene adsorbed on both substrates consist of only one symmetric peak. On copper, this peak appears at a 0.4 eV lower binding energy (BE) than on silver.

Azulene on Ag(111) shows a broad signal with a shoulder at the low binding energy side. This peak shape originates from the chemically different 5- and 7-membered rings, as has been shown by comparison of multilayer XPS data with calculations of the free molecule.²² The fact that the chemical difference of the rings still determines the peak shape in the monolayer is a further indication of a weak interaction of azulene with Ag(111).

On Cu(111), the situation is quite different: The C 1s signal of azulene has lost its shoulder and has acquired a pronounced asymmetry with high-BE tailing, which hints at a hybridization between molecular orbitals and electronic states of the surface. This hybridization leads to the presence of electron density of states around the Fermi edge, which in turn causes the peak asymmetry.⁵² The peak maximum has shifted by 0.7 eV to lower BE, compared to the position on Ag(111). This shift may at least partially be caused by transfer of electron density from the surface to the molecule. In addition, the small adsorption height of azulene on Cu(111) should result in increased final-state screening, which can also contribute to the lowered BE.

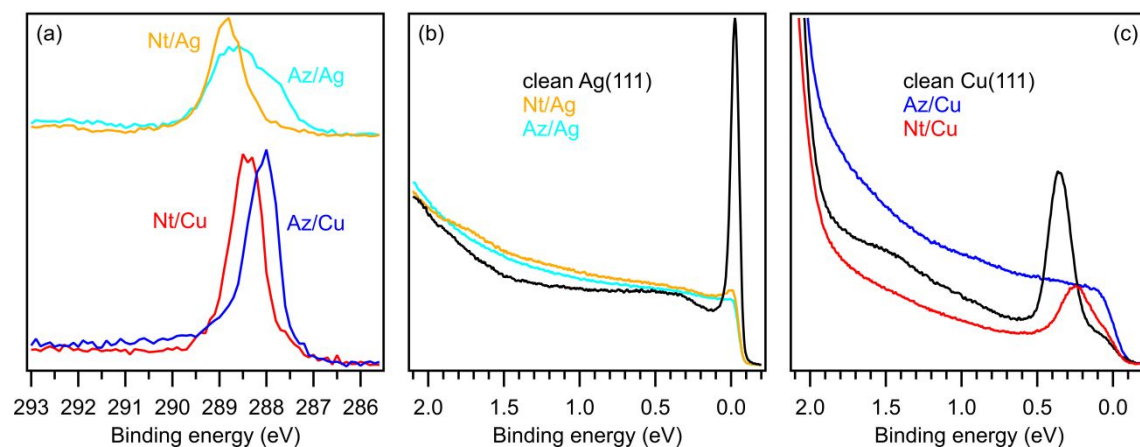


Figure 3. Photoemission spectroscopy of the azulene (Az) and naphthalene (Nt) monolayers on Ag(111) and Cu(111). (a) C 1s XP spectra measured with a photon energy of 600 eV in grazing emission geometry (87° to surface normal). The spectra are normalized with respect to the substrate background at 284 eV. (b) He-I UP spectra for azulene and naphthalene on Ag(111). (c) He-II UP spectra for azulene and naphthalene on Cu(111). All UP spectra were measured in normal emission geometry. The different photon energies for the UP spectra were chosen to avoid substrate satellites in the regions of interest. See Figure S2 in the SI for the spectra taken with the complementary photon energies.

UV photoelectron spectra provide direct insight in the valence electronic structure. In Figure 3b,c, the He-I and He-II UP spectra corresponding to the C 1s data are shown. On Ag(111), adsorption of azulene and naphthalene causes a shift of the surface state to lower BE, leading to its complete disappearance in the case of azulene and only a small residual signal for naphthalene. On Cu(111), naphthalene induces a similar shift of the surface state by 0.1 eV to lower binding energies. In the case of azulene on Cu(111), the surface state is completely suppressed and the whole range between the Fermi edge and copper d-band

shows increased intensity. This behavior was repeatedly observed with different photon energies in different experimental setups and is clearly not due to a normalization error or related issues.

The different influence of the molecules on the surface state of Cu(111) is apparent in the 2D representation of the coverage dependent He-I UPS data presented in Figure 4. For naphthalene on Cu(111), the surface state shifts between 0.1 and 0.2 eV before a coverage of 1.5 ML is reached, after which it is only attenuated with further increase of the coverage. In contrast, the adsorption of azulene on Cu(111) leads to a complete disappearance of the surface state before a coverage of 0.5 ML is reached (Figure 4a). It is then replaced by a broad region of increased intensity (visible also in Figure 3c), which is then attenuated when multilayers are adsorbed. Related UP spectra for a larger energy range show the emergence of molecular states at higher coverages (Figure S3).

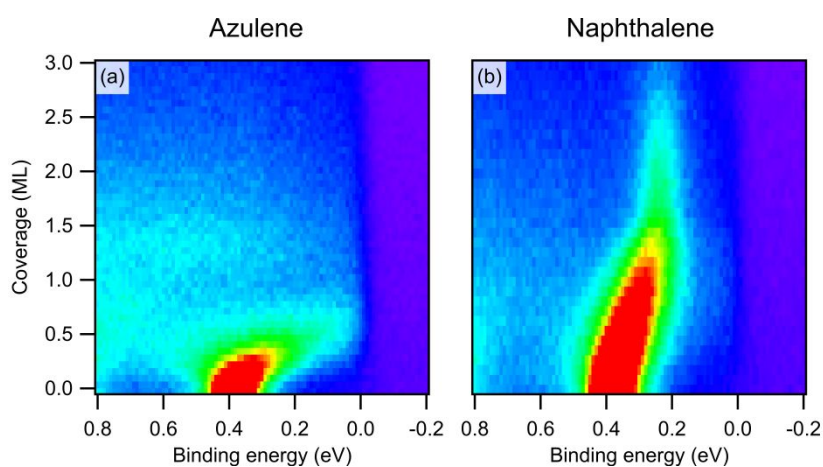


Figure 4. 2D representations of coverage dependent He-I UPS data for (a) azulene and (b) naphthalene on Cu(111). Intensity scale from purple (lowest) to red (highest) in the order of the spectral colors. Extended plots for these measurements and data for the Ag(111) substrate can be found in Figure S3 of the SI.

Unoccupied electronic states: NEXAFS

The unoccupied range of the valence electronic structure was probed with NEXAFS spectroscopy at the carbon K-edge. The resulting spectra for multilayers and monolayers on Ag(111) and Cu(111) are displayed in Figure 5 and compared with DFT calculations.

The multilayer spectra are well reproduced by the calculations, both in the π^* and the σ^* range. Compared to the multilayer, the monolayer of azulene on Ag(111) shows significant broadening and reduction in intensity of the π^* resonance. For naphthalene on Ag(111), the broadening is less pronounced. This is also backed by the corresponding calculations and is an indication for a stronger interaction of azulene.

On Cu(111), the situation of naphthalene is similar to that on Ag(111), whereas in the case of azulene the π^* resonances experience dramatic changes compared to the multilayer spectrum and form now a broad feature with much lower intensity. The reasons for this

deviating behavior of azulene on Cu(111) are discussed later using an advanced projection scheme for the DFT calculations.

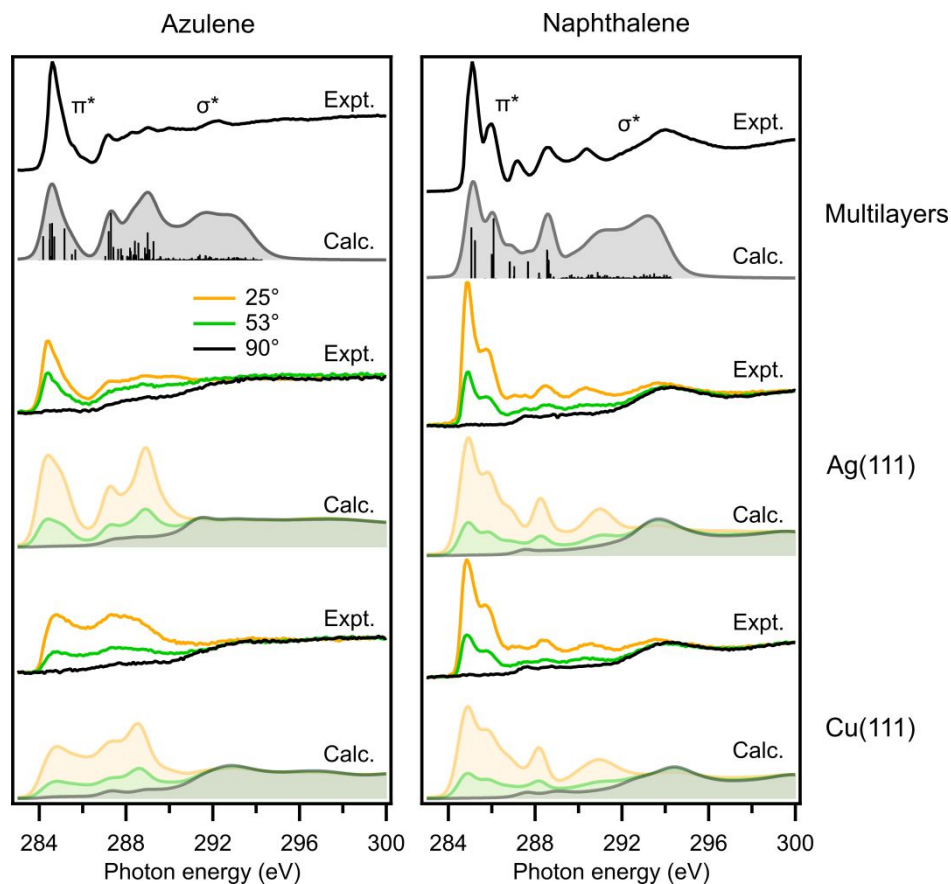


Figure 5. Experimental (Expt.) carbon K-edge NEXAFS spectra and corresponding DFT calculations (Calc.) for azulene and naphthalene. Upper part: Multilayer spectra and calculations for the free molecules. The multilayer spectra were taken with the electric field vector oriented 90° relative to the surface normal. Middle part and lower part: Monolayer spectra and calculations on Ag(111) and Cu(111), respectively, with the different angles of the electric field vector relative to the surface normal as indicated by the color scheme. The calculations for the free molecules are displayed both as isolated excitations and after broadening; the calculations for the monolayers are only shown in broadened form. For the broadening, each excitation is represented by a pseudo-Voigt peak with an increasing width and Lorentzian contribution at higher photon energies. The calculated spectra were rigidly shifted by -6.1 eV to match the experimental energy scale. The data for the copper substrate has already been published elsewhere and is shown again here for direct comparison.²²

Work function changes

Adsorption-induced changes of the electronic work function (WF) of the substrate are related to the vertical dipole moment of the adsorbate-substrate complex. In Figure 6, the experimental WF changes as determined by He-I UPS measurements are plotted as functions of coverage and compared to the DFT-calculated WF changes. The experimental data was fitted with the Topping model⁵³⁻⁵⁴ to extract the unattenuated dipole moment per

molecule μ_0 and the polarizability volume α . Details about the fitting procedure are provided in the SI along with the fits themselves (Figure S4). The parameters obtained by the fits are summarized together with the WF change at monolayer coverage in Table 2.

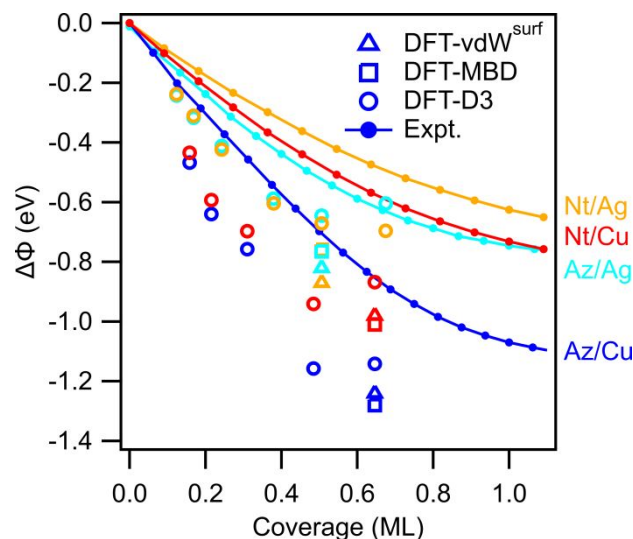


Figure 6. Compilation of the experimental and theoretical results for the work function changes for different coverages of azulene (Az) and naphthalene (Nt). Colors and symbols as labeled in the graph.

Table 2. Work function changes at monolayer coverages of azulene (Az) and naphthalene (Nt), the unattenuated dipole moment $|\mu_0|$ per molecule, and the polarizability volume α as determined by the Topping equation for all four systems.

	Az/Cu	Nt/Cu	Az/Ag	Nt/Ag
$\Delta\Phi$ / eV	-1.07	-0.75	-0.74	-0.63
$ \mu_0 $ / D	2.04	1.35	1.58	1.08
α / 10^{-29} m ³	2.17	1.90	2.70	1.58

The WF change at monolayer coverage is by far the largest for azulene on Cu(111) with -1.07 eV. Azulene on Ag(111) and naphthalene on Cu(111) have almost the same value of -0.74 and -0.75 eV, whereas naphthalene on Ag(111) has the lowest value with -0.63 eV. These same trends hold at submonolayer coverages, while naphthalene/Cu and azulene/Ag have a very similar WF change at higher coverages (Figure 6). The lowering of the work function in all these systems can be attributed to the so called Pauli-pushback effect.⁵⁵⁻⁵⁶ This effect is strongest for azulene on Cu(111) because of its small adsorption height, as determined by NIXSW. As a result, the close proximity between molecule and surface leads to increased repulsion between the electrons in the molecule and the surface. The dipole moments from the Topping fit show the same trend, naphthalene on Cu(111) now has an appreciably lower value than azulene on Ag(111). This result of the fit is to be expected, as it quantifies the behavior of the work function at low coverages, where the

1
2
3 gradient for azulene on Ag(111) is steeper. However, in light of the uncertainties in the
4 experiment the differences between Az/Ag and Nt/Cu are not significant. The comparison
5 between experiment and DFT results will be discussed below.
6
7
8
9

10 **Density-functional theory (DFT) calculations**

11 The experimental data for the two metal surfaces reveal that azulene interacts more strongly
12 with both substrates than its isomer naphthalene. For a detailed understanding of the
13 bonding situation between adsorbate and substrate, DFT calculations were performed.
14 Considering that the correct quantitative description of the van der Waals contribution to
15 the molecule-metal interaction is still challenging,⁵⁷ we compare here four different
16 methods of dispersion correction of the PBE functional in the context of the obtained
17 adsorption heights and the work function changes. The performance of these methods with
18 respect to the adsorption energies will be discussed in a forthcoming paper.
19
20
21
22

23 *Adsorption heights:* To determine the adsorption height D^H , structural optimizations with
24 all methods of dispersion correction were carried out for the $(2\sqrt{3}\times 2\sqrt{3})\text{-}R30^\circ$ structure.
25 The adsorption heights of the molecules were then calculated with respect to the bulk-
26 truncated surface layer to provide the best comparability with the NIXSW measurements.
27 For the theoretical investigation of the coverage-dependence of the adsorption heights,
28 additional calculations were performed only with the DFT-D3 scheme for several other
29 coverages. Note that the range of very low coverages is experimentally increasingly
30 difficult to access, because the resulting signal intensities in the NIXSW experiments get
31 too low, whereas the high coverages are not accessible by theory because no commensurate
32 structures are possible anymore.
33
34
35
36

37 Table 3 and Figure 7 show a generally satisfactory performance of the different theoretical
38 approaches in the overlapping coverage range between theory and experiment. All methods
39 correctly predict that azulene/Cu(111) has (by far) the smallest adsorption height and that
40 naphthalene/Ag(111) has the largest adsorption height. Only MBD correctly predicts the
41 adsorption height of azulene/Ag to be larger than that of naphthalene/Cu. All methods
42 show a comparable average error of 0.04 to 0.07 Å. It is noticeable that vdW^{surf} always
43 gives the smallest adsorption heights of all methods, whereas D3^{surf} and MBD often show
44 the largest adsorption heights. Because of the finite temperature of the measurements
45 combined with the anharmonicity of the molecule-surface potential, the calculated
46 adsorption heights should be slightly smaller than the experimental values, but this effect
47 is within the margin of error.⁵⁸
48
49
50
51
52

53 The coverage-dependent DFT-D3 adsorption heights, also plotted together with the
54 experimental data in Figure 7, show a good agreement with the experimentally observed
55 trends, especially in the case of the Cu surface.
56
57
58
59
60

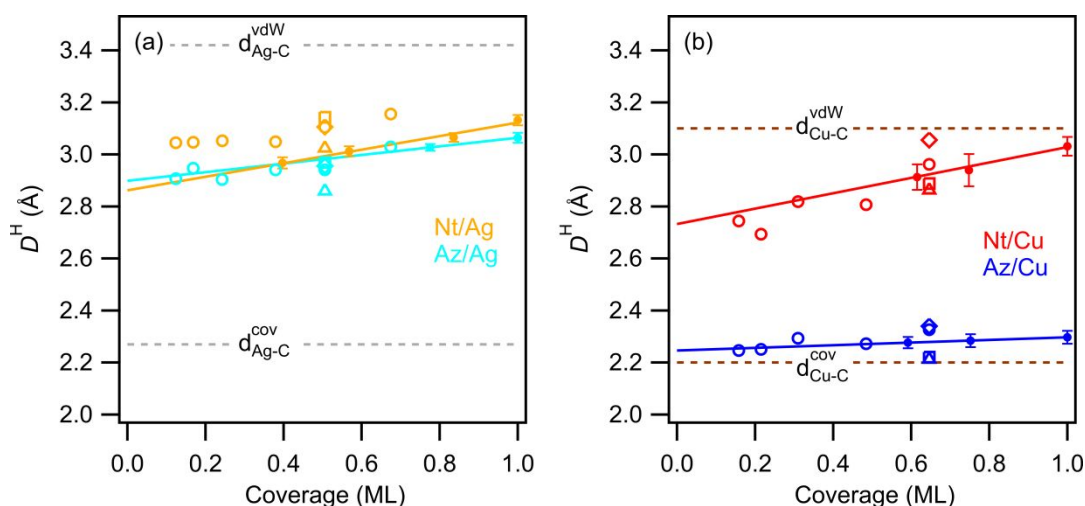


Figure 7. Compilation of the experimental and theoretical results for the adsorption heights of azulene (Az) and naphthalene (Nt) for different coverages, (a) on Ag(111) and (b) on Cu(111). Small filled circles with error bars, experimental data; lines, fit of the experimental data; open circles, D3; triangles, vdW^{surf}; squares, MBD; diamonds, D3^{surf}. The adsorption heights for the $(2\sqrt{3}\times 2\sqrt{3})\text{-}R30^\circ$ structure (0.65 ML on Cu(111) and 0.51 ML on Ag(111)) can be found in Table 3. The horizontal dashed lines indicate the corresponding vdW and covalent distances calculated from literature vdW⁴⁶ and covalent²⁰ radii.

Table 3. Comparison of the experimental (Expt.) values for the adsorption heights D^H of azulene (Az) and naphthalene (Nt) with results calculated using DFT combined with different vdW methods. Note that the coverage for the computational setup is 0.65 ML on Cu(111) and 0.51 ML on Ag(111) corresponding to the $(2\sqrt{3}\times 2\sqrt{3})\text{-}R30^\circ$ structure on both surfaces. The experimental value for the same coverages is calculated using a linear fit of the experimental data points at the measured coverages.

D^H in Å	Az/Cu	Nt/Cu	Az/Ag	Nt/Ag
Expt.	2.28	2.92	2.98	2.99
D3	2.33	2.96	2.94	3.10
vdW ^{surf}	2.21	2.86	2.86	3.02
MBD	2.22	2.89	2.97	3.14
D3 ^{surf}	2.34	3.06	2.96	3.11

Work function changes: Comparison of the experimental WF changes with those obtained by DFT (Table 4 and Figure 6) reveal more pronounced differences. All theoretical methods overestimate the WF change in all cases. This is probably due to the shortcomings of the PBE functional and the influence of the finite temperature. Consistent with the pushback effect, the adsorption geometry is expected to have a strong impact on the WF; methods that yield a small adsorption height show a large WF reduction, whereas a larger adsorption height correlates with a smaller WF reduction. Hence, the observed differences between the methods arise to some extent from the different adsorption height predicted by

them. The order (trends) in the WF changes between the different systems are correctly reproduced by all methods, with the only exception that all methods yield a large overestimation in the case of naphthalene on Ag(111).

Table 4. Comparison of the experimental work function changes (Expt.) of azulene (Az) and naphthalene (Nt) with results obtained from DFT calculations with different vdW methods. The work functions were calculated with the adsorption geometries pertinent to each method. Note that the coverage is 0.65 ML on Cu(111) and 0.51 ML on Ag(111) corresponding to the $(2\sqrt{3}\times 2\sqrt{3})\text{-}R30^\circ$ structure on both surfaces. To get an experimental value at these coverages, the work function change was linearly interpolated between the two closest data points.

$\Delta\Phi$ in eV	Az/Cu	Nt/Cu	Az/Ag	Nt/Ag
Expt.	-0.86	-0.58	-0.53	-0.40
D3	-1.14	-0.87	-0.65	-0.67
vdW ^{surf}	-1.24	-0.98	-0.82	-0.87
MBD	-1.28	-1.01	-0.76	-0.76

Charge density difference plots: The charge redistribution between surface and molecule is indicative for the nature of the adsorbate-substrate interactions. Analysis of the charge density difference plots (Figure 8) reveals multiple effects: (1) Just above the first surface layer, electrons are depleted in the space beneath each molecule and enriched in the areas in-between molecules. This charge redistribution is attributed to the Pauli pushback effect.⁵⁵⁻⁵⁶ (2) Charge is enriched halfway between molecule and surface indicating a bonding interaction. The effects (1) and (2) are, on the same surface, stronger for azulene than for naphthalene, and on Cu(111) stronger than on Ag(111). They are strongest for azulene on Cu(111), where an additional effect occurs: (3) Charge transfer from the surface into the former LUMO of the molecule. This charge flow can be seen at a much larger iso-value (see Figure S5 in the SI) and was already reported in previous work.²²

To summarize, on silver both molecules show a redistribution pattern consistent with the push-back effect accompanying physisorption, with the effect being stronger for azulene (Figure 8a,b) than for naphthalene (Figure 8c,d). On copper, naphthalene shows the same physisorptive behavior but in a more pronounced way (Figure 8g,h), whereas azulene and the surface experience a massive charge redistribution (Figure 8e,f) and an additional charge transfer from the surface to the molecule.

Regarding the overall resulting vertical dipole moment for azulene on Cu(111), the push-back effect overcompensates the contribution of the surface-to-molecule charge transfer. As a result, the dipole moment remains in all cases oriented antiparallel to the surface dipole of the clean surface and the work function is therefore reduced, as already seen in the UPS results above.

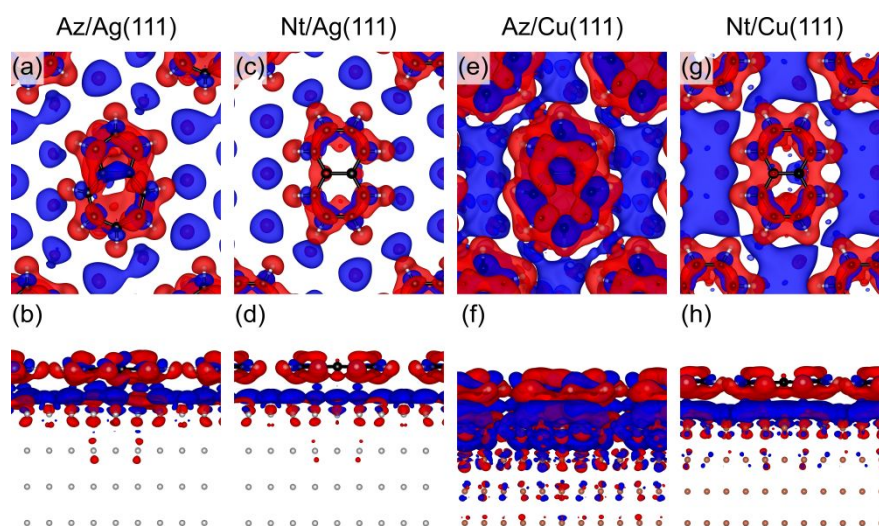


Figure 8. Top and side views of the charge density difference plots for of azulene (Az) and naphthalene (Nt) on Ag(111) and Cu(111). The isosurface value is $0.0005 \text{ e}/\text{\AA}^3$ for all plots. Blue, electron accumulation; red, electron depletion.

The DFT-D3 values of the unattenuated vertical dipole moment μ_0 were obtained by fitting the dipole moments of the different coverages using a modified Topping equation.⁵³⁻⁵⁴ The resulting μ_0 values are compared to the corresponding experimental values in Table 5, revealing substantial overestimation by the computational method used. This is not surprising, as the (independently calculated) WF changes were also overestimated by theory. The experimental trend is reproduced correctly with the exception of a large deviation for Nt/Cu.

Table 5. Comparison between the vertical dipole moments $|\mu_0|$ of azulene (Az) and naphthalene (Nt) calculated by DFT-D3 and experimental values obtained from the work function change measured by UPS. All theoretical and experimental values are extrapolated to the zero coverage limit and were determined by a Topping fit of the coverage dependent measurements and calculations.

$ \mu_0 $ in D	Az/Cu	Nt/Cu	Az/Ag	Nt/Ag
$ \mu_0 $ (UPS)	2.04	1.35	1.58	1.08
$ \mu_0 $ (DFT)	3.77	3.64	2.37	1.61

To quantify the charge transfer between molecule and substrate, two different charge partitioning schemes were employed. These are the atoms-in-molecules (AIM) charge analysis developed by Bader⁵⁹ and the integration of the molecular DOS up to the Fermi energy. Both reveal that significant total surface-to-molecule charge transfer occurs only for azulene on Cu(111). For the other systems, the obtained total charges are not of a significant magnitude compared to the typical deviations of DFT partial charges. However,

this does not mean that there is no local adsorption-induced charge redistribution in these systems, as can be seen in the charge density difference plots (Figure 8).

Table 6. Comparison of the total charge transfer q from surface to of azulene (Az) and naphthalene (Nt), as calculated by AIM charge analysis and by integrating the molecular projected DOS up to E_F . A negative sign means charge is transferred from the substrate to the molecule. The charges for the adsorbates on copper have already been published in previous work.²²

q in e	Az/Cu	Nt/Cu	Az/Ag	Nt/Ag
q_{AIM}	-0.49	0.06	0.01	0.06
q_{DOS}	-1.39	-0.13	-0.21	-0.05

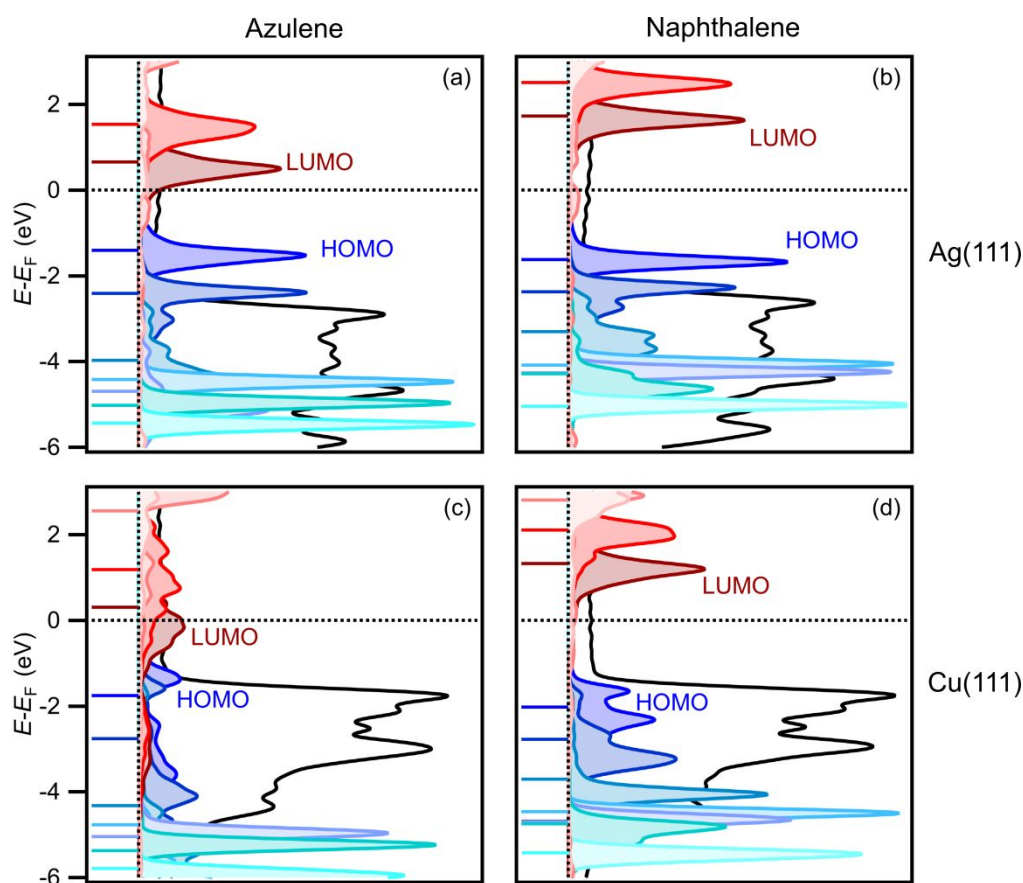


Figure 9. DFT calculated density of states (DOS) of the adsorbed species. MO-projected DOS for (a) azulene on Ag(111), (b) naphthalene on Ag(111), (c) azulene on Cu(111), (d) naphthalene on Cu(111). Contributions of the LUMO in dark red and those of the HOMO in blue; higher or lower orbitals in incrementally lighter colors. In addition, the total density of states (in black, scaled for better presentation) and the energies of the molecular frontier orbitals (shown as horizontal lines) are included. The data for the copper substrate has already been published elsewhere and is shown again here for direct comparison.²²

Molecular-orbital projection scheme: The valence electronic structure of the adsorbed molecules can also be analyzed by a MO projection scheme, which reveals the adsorption-induced changes of the molecular orbitals. As shown in Figure 9, there are substantial differences of the energetic position of the frontier orbitals. Due to the lower HOMO-LUMO gap of azulene, its frontier orbitals are closer to the Fermi energy (E_F) of the metal. On Ag(111), these orbitals experience a somewhat larger broadening in the case of azulene compared to naphthalene, especially the LUMO and LUMO+1 orbitals. On Cu(111), the situation is more pronounced and the DOS contribution of the LUMO and the LUMO+1 of azulene are substantially broadened, resulting in large contributions of the former unoccupied orbitals below E_F . The presence of this very broad state around E_F is also in agreement with the UP spectra in Figures 3 and 4. For naphthalene on Cu(111) the frontier orbitals are only slightly more broadened than on Ag(111) and do not have significant contributions below E_F .

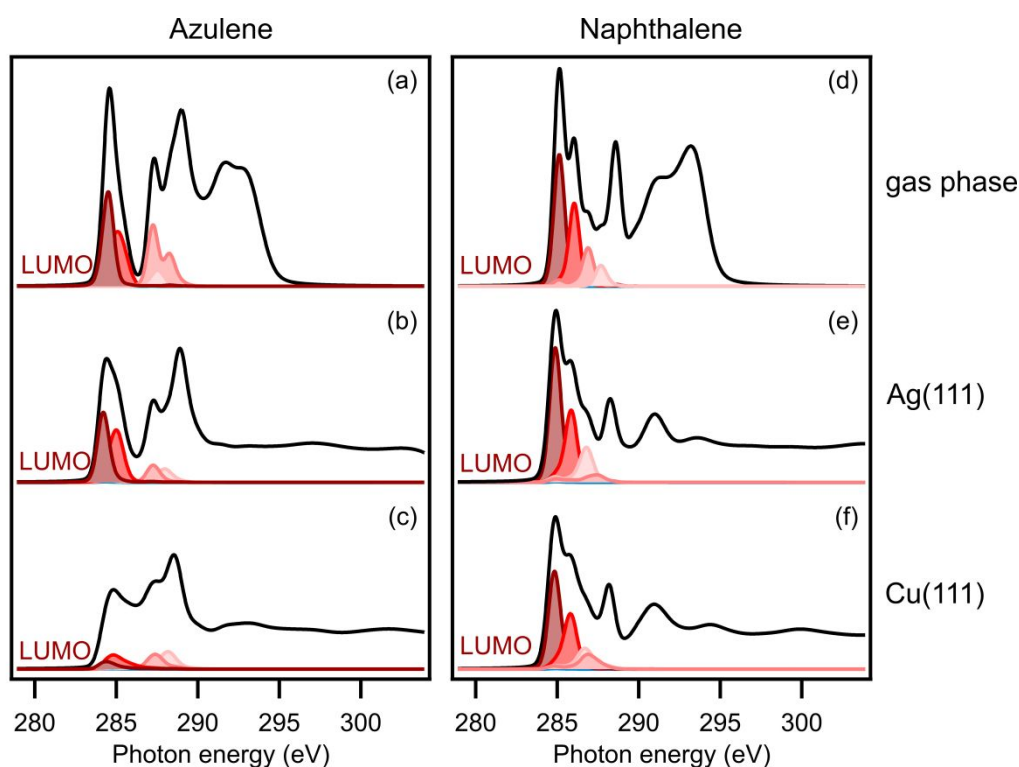


Figure 10. MO projection analysis of the NEXAFS spectra, left azulene, right naphthalene. Contributions of the LUMO in dark red, higher orbitals in incrementally lighter colors, total spectrum in black. (a, d) MO-projected NEXAFS calculations of the free molecules. MO-projected NEXAFS calculations (25° incidence) of the molecules adsorbed on Ag(111) (b, e) and on Cu(111) (c, f). The calculated spectra were shifted by -6.1 eV to match the experimental energy scale. The data for the copper substrate has already been published elsewhere and is shown again here for direct comparison.²²

NEXAFS calculations: For a detailed theoretical analysis of the NEXAFS spectra, we calculated the contribution of the molecular orbitals of the free azulene and naphthalene molecules to the calculated NEXAFS spectra. Hereby, the overlap between the ground-state molecular orbitals of the free molecules with the final-state corrected transition potential wavefunctions has been calculated. As can be seen in Figure 10, the first π^* resonance comprises contributions from the LUMO and LUMO+1 for both molecules. The calculations further reveal the influence of the substrate on the NEXAFS transitions. Compared to the free molecule, azulene on Ag(111) shows a broadening of the π^* resonance caused by a shift of the transition involving the LUMO to lower photon energies, while the LUMO+1 contribution stays at the same position. For naphthalene no such shift is visible and the broadening is less pronounced. For azulene on Cu(111) the situation becomes extreme and the contributions of these two orbitals are substantially reduced, leading to a strong change in spectral appearance. Naphthalene on the other hand does not experience a major change in the total NEXAFS signal or the contributing transitions and the spectra of the free molecule and the adsorbed species on Cu(111) and on Ag(111) are similar. From these results, it is concluded that the electronic structure of naphthalene is not significantly influenced by either substrate. In contrast, azulene experiences substantial influence on the LUMO already when adsorbed on Ag(111), while adsorption on Cu(111) causes a massive reduction in intensity of the π^* resonance, indicating a complete change in the electronic structure and a partial filling of the LUMO and LUMO+1 orbitals, in line with previous work.²²

DISCUSSION

The experimental and computational results presented above show unambiguously that the nonalternant π -electron system of azulene results in a stronger interaction with both metal surface at all investigated coverages. In the following, we discuss how the interaction with the surface influences the aromatic character of the molecules. The partial occupation of formerly unoccupied molecular orbitals, as observed in the NEXAFS measurements, should lead to increased C-C bond lengths in the adsorbed molecules. Indeed, the DFT calculation show that all bonds of naphthalene and most bonds of azulene are elongated in the adsorbed structures. There only exception is the bridging C-C bond in azulene, which is substantially shortened both on Ag(111) and (even more pronounced) on Cu(111). This different pattern of bond-length change of azulene and naphthalene can be rationalized within the concept of aromaticity. A prerequisite of this approach is that the sp^2 -to- sp^3 rehybridisation accompanying the adsorption is weak enough, which seems fulfilled as the out-of-plane angles are only about 10° for azulene on Cu(111) as the most strongly interacting system and less than 2° for all other systems.

A widely used method to quantify aromaticity is the harmonic oscillator model of aromaticity (HOMA)⁶⁰, which is based on the molecular geometry and takes the deviation of the bond lengths from the ideal aromatic bond into account. The model parameters R_{opt} (the optimal C-C bond length of the reference molecule) and α are chosen such that the

1
2
3 benzene molecule (with six equally long bonds) has a HOMA value of 1, whereas the
4 hypothetical Kekulé-like benzene (with three single and three double bonds) has a HOMA
5 value of 0. For the HOMA values discussed below, we used the bond lengths obtained from
6 the DFT-optimized structures, the parameters used to calculate the HOMA values stem
7 from free benzene optimized with the same method ($R_{\text{opt}} = 1.398 \text{ \AA}$ and $\alpha = 362.1 \text{ \AA}^{-2}$).
8
9

10 For molecules with more than one ring, different HOMA values can be calculated,
11 depending on which π -bonds and conjugation paths are taken into account. One possibility
12 is to use all π -bonds in the molecule; this will be denoted as overall HOMA value O. If
13 only the perimeter π -bonds of the molecule are used, this is called the perimeter HOMA
14 value P. In addition, the HOMA value R for each ring can be calculated separately. Figure
15 11a shows all these HOMA values for azulene and naphthalene as well as the reference
16 molecule benzene in their gas phase structure as well as adsorbed on Ag(111) and Cu(111).
17 For convenience, we introduce here the *Excess Perimeter Conjugation* $\text{EPC} = \text{P} - \text{O}$. This
18 parameter provides a simple way to express the degree of annulenoid versus benzenoid
19 aromaticity⁶¹ within the HOMA concept. For a molecule with annulene character, *i.e.*,
20 when the aromatic conjugation is predominantly along its perimeter (annulenoid
21 aromaticity⁶¹), the EPC value is large. In contrast, a small EPC value means that the
22 conjugation is distributed over the whole molecule (benzenoid aromaticity⁶¹). A higher
23 EPC value therefore means a more annulene-like conjugation in the molecule, as illustrated
24 in Figure 11b. For the free molecules, it is obvious that naphthalene ($\text{EPC} = 0.04$) shows
25 conjugation over the whole molecule (predominant benzenoid aromaticity). Azulene,
26 however, shows a high annulene-like character ($\text{EPC} = 0.32$, predominant annulenoid
27 aromaticity). This conclusion derived from the HOMA values is in agreement with the
28 extremely elongated bridging bond in the azulene molecule and also with a topological
29 analysis of the aromaticity performed by Aihara.⁶²⁻⁶³
30
31
32
33
34
35
36
37
38

39 Figure 11a shows that, for benzene and naphthalene, the conjugation does not change when
40 they are adsorbed on Ag(111) or Cu(111). This result is not surprising, because these
41 molecules are only weakly physisorbed. For azulene the situation is different: On Ag(111),
42 it shows already a more benzenoid aromaticity ($\text{EPC} = 0.24$) and the HOMA values of both
43 rings increase. On Cu(111), the character of the conjugation gets even closer to the level of
44 naphthalene ($\text{EPC} = 0.11$). The change away from annulenoid aromaticity for the adsorbed
45 molecule is also visible in the bond lengths: The bridging bond in azulene gets slightly
46 shorter when adsorbed on Ag(111) and even shorter when adsorbed on Cu(111). The other
47 bonds in azulene get longer when adsorbed on Cu(111) leading to an overall decrease of
48 the HOMA values compared to adsorption on Ag(111). (However, the HOMA values of
49 both rings in azulene/Cu are still increased relative to those of the free molecule.) These
50 considerations show that the metal surface promotes a change from the annulenoid
51 aromaticity of the free azulene molecule to a more benzenoid aromaticity, via transfer of
52 electron density into previously unoccupied orbitals.
53
54
55
56
57
58
59
60

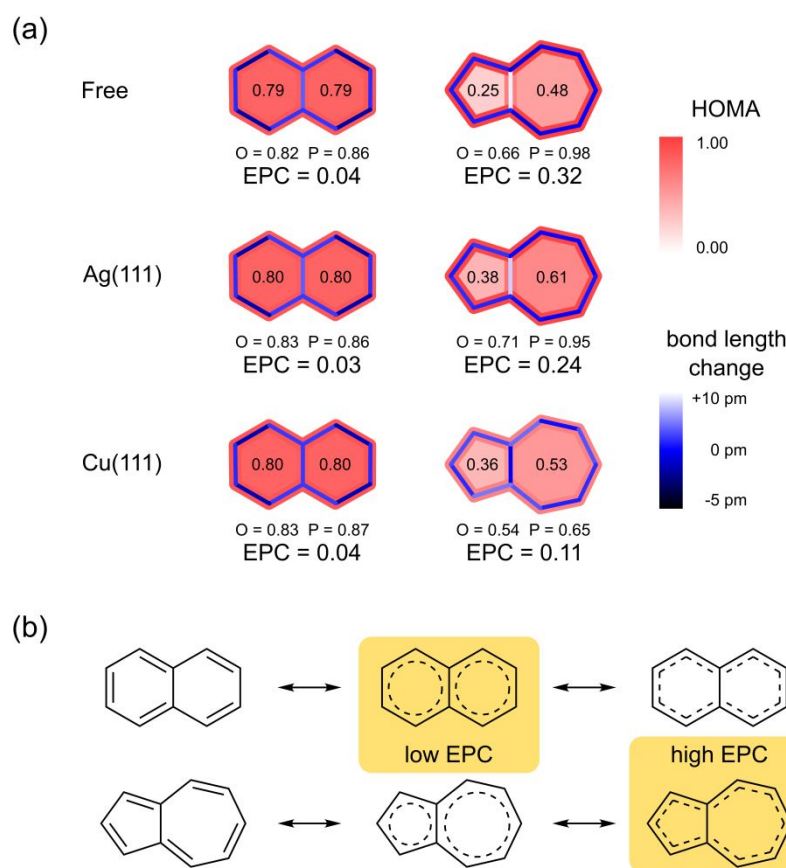


Figure 11. (a) HOMA analysis for azulene and naphthalene in the gas phase and adsorbed on Ag(111) and Cu(111), based on the DFT-optimized structures. The red color scheme shows the HOMA value. The fill color of each ring represents its HOMA value (R), the perimeter bonds are colored according to the perimeter HOMA value (P), and the bridging bonds are colored according to the overall HOMA value (O). All bonds are additionally colored with a blue color scheme representing the bond-length change with respect to the ideal aromatic bond. For the definition of EPC, see the text. (b) Comparison of the regular Lewis structures (left) with resonance structures indicating predominant benzenoid aromaticity (low EPC, center) of naphthalene and predominant annulenoid aromaticity (high EPC, right) of azulene.

CONCLUSION

Comparison of the isomers azulene and naphthalene reveals that the topology of the π -electron system has a strong influence on the interaction with metal surfaces. Azulene with its pentagon-heptagon ring system forms stronger bonds to both Ag(111) and Cu(111) than naphthalene. Coverage-dependent measurements of the vertical bond distances (adsorption heights) with NIXSW show that azulene forms shorter bonds than naphthalene on both surfaces at all investigated coverages. The shortest distances were measured for azulene/Cu (*e.g.* 2.28 Å at 0.75 ML), which is only slightly longer than a covalent C-Cu bond in organometallic compounds. The corresponding value for naphthalene is much larger (2.94 Å at 0.75 ML). On Ag(111), the differences are significant but smaller (0.04-0.07 Å). The C 1s XP spectra of monolayers show characteristic differences between azulene and

naphthalene. The dipolar nature of azulene is reflected in an increased peak width on Ag, while on Cu the azulene signal changes shape and position, indicating substantial electron transfer from the surface to the molecule. Valence photoemission spectra show increased intensity below E_F especially for azulene/Cu, while the surface state is differently affected by azulene and naphthalene. On both metals, azulene induces larger work function reductions and creates stronger surface dipoles than naphthalene. NEXAFS reveals substantial differences also in the unoccupied valence range. The shape of the π^* resonance is more affected by adsorption in the case of azulene. Especially for azulene/Cu, the π^* resonance is substantially attenuated and broadened, in line with a strong hybridization and partial occupation of the former LUMO. DFT calculations using four different methods of dispersion correction of the PBE functional (the DFT-D3 scheme with Becke-Johnson damping function, the vdW^{surf} correction based on DFT-TS, a Many-Body Dispersion (MBD) correction scheme, and the D3^{surf} scheme) all provide a good agreement with the experimental adsorption heights. Additional calculations with the DFT-D3 scheme reproduce the coverage dependence of the adsorption height reasonably well. WF changes are overestimated by the PBE functional regardless of the dispersion correction that was used to optimize the adsorption structure. AIM analysis reveals substantial surface-to-molecule electron transfer for azulene/Cu (-0.49 e), whereas the charge transfer for the other systems is negligible (0.01 to 0.06 e); an alternative charge partitioning scheme substantiates this finding. Due to its nonalternant topology and the corresponding small HOMO-LUMO gap, the LUMO of azulene is much closer to E_F of both metals than the LUMO of naphthalene. As a result, the LUMO of azulene hybridizes with the wave functions of the metal surfaces, as revealed by calculations of the MO-projected density of valence states. This effect is especially pronounced for azulene/Cu. MO projection analysis of the NEXAFS spectra proves that this hybridization is also responsible for the adsorption-related changes of the first π^* resonance, which is dominated by the contributions of the LUMO and LUMO+1. The interaction with the metal substrates can also affect the aromaticity of the molecule. In the case of azulene, it promotes a change from the annulenoid character of the free azulene molecule to a more benzenoid character. Overall, our results reveal the critical role of molecular topology in controlling the chemical bond and the electronic interactions at interfaces between π -conjugated ring systems and metal surfaces.

ASSOCIATED CONTENT

Supporting Information.

Supporting information containing details of the DFT calculations, additional NIXSW data and UPS spectra, details about the Topping fit procedure as well as complementary charge density difference plots can be found free of charge at the website of the publisher.

AUTHOR INFORMATION**Corresponding Author**

*michael.gottfried@chemie.uni-marburg.de

Notes

The authors declare no competing financial interest.

ACKNOWLEDGMENT

Funded by the Deutsche Forschungsgemeinschaft through 223848855-SFB1083. We thank the Diamond Light Source for access to beamline I09 (Proposal No. SI16259), and the I09 beam-line staff (T.-L. Lee, P. K. Thakur, and D. McCue) for their excellent support during the experiment. Furthermore we thank the synchrotron radiation facility BESSY-II of the Helmholtz-Zentrum für Materialien und Energie, Berlin, for allocation of beam time at the beam line HE-SGM and financial support. JMM gratefully acknowledges the computing time granted by the John von Neumann Institute for Computing (NIC) and provided on the supercomputer JURECA⁶⁴ at Jülich Supercomputing Centre (JSC). We further acknowledge computational resources from HLR Stuttgart, CSC-LOEWE Frankfurt, and HRZ Marburg. SJH and RJM acknowledge funding for a PhD studentship through the EPSRC Centre for Doctoral Training in Molecular Analytical Science (EP/L015307/1) and computing resources via the EPSRC-funded HPC Midlands+ computing centre (EP/P020232/1) and the EPSRC-funded Materials Chemistry Consortium for the ARCHER UK National Supercomputing Service (EP/R029431/1). RJM acknowledges support via a UKRI Future Leaders Fellowship (MR/S016023/1).

REFERENCES

1. Witte, G.; Wöll, C. Growth of Aromatic Molecules on Solid Substrates for Applications in Organic Electronics. *J. Mater. Res.* **2011**, *19*, 1889-1916.
2. Facchetti, A. π -Conjugated Polymers for Organic Electronics and Photovoltaic Cell Applications. *Chem. Mater.* **2011**, *23*, 733-758.
3. Wu, J.; Pisula, W.; Müllen, K. Graphenes as Potential Material for Electronics. *Chem. Rev.* **2007**, *107*, 718-747.
4. Burroughes, J. H.; Bradley, D. D. C.; Brown, A. R.; Marks, R. N.; Mackay, K.; Friend, R. H.; Burns, P. L.; Holmes, A. B. Light-Emitting Diodes Based on Conjugated Polymers. *Nature* **1990**, *347*, 539-541.
5. Forrest, S. R. The Path to Ubiquitous and Low-Cost Organic Electronic Appliances on Plastic. *Nature* **2004**, *428*, 911-918.
6. *Organic Electronics: Materials, Manufacturing, and Applications*; Klauk, H., Ed.; Wiley-VCH: Weinheim, **2006**.
7. *Organic Electronics II: More Materials and Applications*; Klauk, H., Ed.; Wiley-VCH: Weinheim, **2012**.
8. Koch, N. Organic Electronic Devices and Their Functional Interfaces. *ChemPhysChem* **2007**, *8*, 1438-1455.
9. Cusati, T.; Fiori, G.; Gahoi, A.; Passi, V.; Lemme, M. C.; Fortunelli, A.; Iannaccone, G. Electrical Properties of Graphene-Metal Contacts. *Sci. Rep.* **2017**, *7*, 5109.
10. Hwang, J.; Wan, A.; Kahn, A. Energetics of Metal–Organic Interfaces: New Experiments and Assessment of the Field. *Mater. Sci. Eng. R Rep.* **2009**, *64*, 1-31.
11. Scott, J. C. Metal–Organic Interface and Charge Injection in Organic Electronic Devices. *J. Vac. Sci. Technol. A* **2003**, *21*, 521-531.
12. Gottfried, J. M. Quantitative Model Studies for Interfaces in Organic Electronic Devices. *New J. Phys.* **2016**, *18*, 111002.
13. Kahn, A.; Koch, N.; Gao, W. Electronic Structure and Electrical Properties of Interfaces between Metals and π -Conjugated Molecular Films. *J. Polym. Sci. B* **2003**, *41*, 2529-2548.
14. Käfer, D.; Ruppel, L.; Witte, G. Growth of Pentacene on Clean and Modified Gold Surfaces. *Phys. Rev. B* **2007**, *75*, 085309.
15. Käfer, D.; Witte, G. Evolution of Pentacene Films on Ag(111): Growth Beyond the First Monolayer. *Chem. Phys. Lett.* **2007**, *442*, 376-383.
16. Tautz, F. S. Structure and Bonding of Large Aromatic Molecules on Noble Metal Surfaces: The Example of PTCDA. *Prog. Surf. Sci.* **2007**, *82*, 479-520.
17. Winter, B.; Ivanco, J.; Netzer, F. P.; Ramsey, M. G.; Salzmann, I.; Resel, R. Epitaxial Growth of Sexiphenyl on Al(111): From Monolayer to Crystalline Films. *Langmuir* **2004**, *20*, 7512-7516.
18. Liu, W.; Maaß, F.; Willenbockel, M.; Bronner, C.; Schulze, M.; Soubatch, S.; Tautz, F. S.; Tegeder, P.; Tkatchenko, A. Quantitative Prediction of Molecular Adsorption: Structure and Binding of Benzene on Coinage Metals. *Phys. Rev. Lett.* **2015**, *115*, 036104.
19. Mallion, R. B.; Rouvray, D. H. The Golden Jubilee of the Coulson-Rushbrooke Pairing Theorem. *J. Math. Chem.* **1990**, *5*, 1-21.
20. *CRC Handbook of Chemistry and Physics*; Lide, D. R., Ed.; 90 ed.; CRC Press: Boca Raton, FL, **2010**.
21. Xin, H.; Gao, X. Application of Azulene in Constructing Organic Optoelectronic Materials: New Tricks for an Old Dog. *ChemPlusChem* **2017**, *82*, 945-956.
22. Klein, B. P.; van der Heijden, N. J.; Kachel, S. R.; Franke, M.; Krug, C. K.; Greulich, K. K.; Ruppenthal, L.; Müller, P.; Rosenow, P.; Parhizkar, S., et al. Molecular Topology and the Surface Chemical Bond: Alternant Versus Nonalternant Aromatic Systems as Functional Structural Elements. *Phys. Rev. X* **2019**, *9*, 011030.
23. Becke, A. D.; Johnson, E. R. A Density-Functional Model of the Dispersion Interaction. *J. Chem. Phys.* **2005**, *123*, 154101.

- 1
 - 2
 - 3
 - 4
 - 5
 - 6
 - 7
 - 8
 - 9
 - 10
 - 11
 - 12
 - 13
 - 14
 - 15
 - 16
 - 17
 - 18
 - 19
 - 20
 - 21
 - 22
 - 23
 - 24
 - 25
 - 26
 - 27
 - 28
 - 29
 - 30
 - 31
 - 32
 - 33
 - 34
 - 35
 - 36
 - 37
 - 38
 - 39
 - 40
 - 41
 - 42
 - 43
 - 44
 - 45
 - 46
 - 47
 - 48
 - 49
 - 50
 - 51
 - 52
 - 53
 - 54
 - 55
 - 56
 - 57
 - 58
 - 59
 - 60
24. Grimme, S.; Ehrlich, S.; Goerigk, L. Effect of the Damping Function in Dispersion Corrected Density Functional Theory. *J. Comput. Chem.* **2011**, *32*, 1456-1465.
25. Ruiz, V. G.; Liu, W.; Zojer, E.; Scheffler, M.; Tkatchenko, A. Density-Functional Theory with Screened Van Der Waals Interactions for the Modeling of Hybrid Inorganic-Organic Systems. *Phys. Rev. Lett.* **2012**, *108*, 146103.
26. Tkatchenko, A.; Scheffler, M. Accurate Molecular Van Der Waals Interactions from Ground-State Electron Density and Free-Atom Reference Data. *Phys. Rev. Lett.* **2009**, *102*, 073005.
27. Lifshitz, E. M. The Theory of Molecular Attractive Forces between Solids. *Soviet Physics JETP* **2** **1956**, *2*, 73-83.
28. Zaremba, E.; Kohn, W. Van Der Waals Interaction between an Atom and a Solid Surface. *Phys. Rev. B* **1976**, *13*, 2270-2285.
29. Tkatchenko, A.; DiStasio, R. A.; Car, R.; Scheffler, M. Accurate and Efficient Method for Many-Body Van Der Waals Interactions. *Phys. Rev. Lett.* **2012**, *108*, 236402.
30. Ambrosetti, A.; Reilly, A. M.; DiStasio, R. A.; Tkatchenko, A. Long-Range Correlation Energy Calculated from Coupled Atomic Response Functions. *J. Chem. Phys.* **2014**, *140*, 18A508.
31. Bocquet, F. C.; Mercurio, G.; Franke, M.; van Straaten, G.; Weiß, S.; Soubatch, S.; Kumpf, C.; Tautz, F. S. TORRICELLI: A Software to Determine Atomic Spatial Distributions from Normal Incidence X-Ray Standing Wave Data. *Comput. Phys. Commun.* **2018**, *235*, 502-513.
32. The latest version of the open-source software TORRICELLI is available at www.torricelli-software.com (accessed Oct 26, 2019).
33. van Straaten, G.; Franke, M.; Bocquet, F. C.; Tautz, F. S.; Kumpf, C. Non-Dipolar Effects in Photoelectron-Based Normal Incidence X-Ray Standing Wave Experiments. *J. Electron Spectrosc. Rel. Phenom.* **2018**, *222*, 106-116.
34. Perdew, J. P.; Burke, K.; Ernzerhof, M. Generalized Gradient Approximation Made Simple. *Phys. Rev. Lett.* **1996**, *77*, 3865-3868.
35. Grimme, S.; Antony, J.; Ehrlich, S.; Krieg, H. A Consistent and Accurate Ab Initio Parametrization of Density Functional Dispersion Correction (DFT-D) for the 94 Elements H-Pu. *J. Chem. Phys.* **2010**, *132*, 154104.
36. Clark, S. J.; Segall, M. D.; Pickard, C. J.; Hasnip, P. J.; Probert, M. I. J.; Refson, K.; Payne, M. C. First Principles Methods Using CASTEP. *Z. Kristallogr. Cryst. Mater.* **2009**, *220*, 567-570.
37. T. Mizoguchi; I. Tanaka; S.-P. Gao; Pickard, C. J. First-Principles Calculation of Spectral Features, Chemical Shift and Absolute Threshold of ELNES and XANES Using a Plane Wave Pseudopotential Method. *J. Phys.: Condens. Matter* **2009**, *21*, 104204.
38. Triguero, L.; Pettersson, L. G. M.; Ågren, H. Calculations of near-Edge X-Ray-Absorption Spectra of Gas-Phase and Chemisorbed Molecules by Means of Density-Functional and Transition-Potential Theory. *Phys. Rev. B* **1998**, *58*, 8097-8110.
39. Klues, M.; Hermann, K.; Witte, G. Analysis of the near-Edge X-Ray-Absorption Fine-Structure of Anthracene: A Combined Theoretical and Experimental Study. *J. Chem. Phys.* **2014**, *140*, 014302.
40. Diller, K.; Maurer, R. J.; Müller, M.; Reuter, K. Interpretation of X-Ray Absorption Spectroscopy in the Presence of Surface Hybridization. *J. Chem. Phys.* **2017**, *146*, 214701.
41. Maurer, R. J.; Reuter, K. Excited-State Potential-Energy Surfaces of Metal-Adsorbed Organic Molecules from Linear Expansion Δ -Self-Consistent Field Density-Functional Theory (Δ SCF-DFT). *J. Chem. Phys.* **2013**, *139*, 014708.
42. Woodruff, D. P. Normal Incidence X-Ray Standing Wave Determination of Adsorbate Structures. *Prog. Surf. Sci.* **1998**, *57*, 1-60.
43. Woodruff, D. P. Surface Structure Determination Using X-Ray Standing Waves. *Rep. Prog. Phys.* **2005**, *68*, 743-798.
44. Zegenhagen, J. Surface Structure Determination with X-Ray Standing Waves. *Surf. Sci. Rep.* **1993**, *18*, 202-271.

- 1
 - 2
 - 3
 - 4
 - 5
 - 6
 - 7
 - 8
 - 9
 - 10
 - 11
 - 12
 - 13
 - 14
 - 15
 - 16
 - 17
 - 18
 - 19
 - 20
 - 21
 - 22
 - 23
 - 24
 - 25
 - 26
 - 27
 - 28
 - 29
 - 30
 - 31
 - 32
 - 33
 - 34
 - 35
 - 36
 - 37
 - 38
 - 39
 - 40
 - 41
 - 42
 - 43
 - 44
 - 45
 - 46
 - 47
 - 48
 - 49
 - 50
 - 51
 - 52
 - 53
 - 54
 - 55
 - 56
 - 57
 - 58
 - 59
 - 60
45. Kröger, I.; Bayersdorfer, P.; Stadtmüller, B.; Kleimann, C.; Mercurio, G.; Reinert, F.; Kumpf, C. Submonolayer Growth of H₂-Phthalocyanine on Ag(111). *Phys. Rev. B* **2012**, *86*, 195412.
46. Bondi, A. Van Der Waals Volumes and Radii. *J. Phys. Chem.* **1964**, *68*, 441-451.
47. Zhao, W.; Wei, W.; White, J. M. Two-Photon Photoemission Spectroscopy: Naphthalene on Cu(111). *Surf. Sci.* **2003**, *547*, 374-384.
48. Rockey, T.; Dai, H.-L. Adsorbate-Substrate Bonding and the Growth of Naphthalene Thin Films on Ag(111). *Surf. Sci.* **2007**, *601*, 2307-2314.
49. Kröger, I.; Stadtmüller, B.; Stadler, C.; Ziroff, J.; Kochler, M.; Stahl, A.; Pollinger, F.; Lee, T.-L.; Zegenhagen, J.; Reinert, F., et al. Submonolayer Growth of Copper-Phthalocyanine on Ag(111). *New J. Phys.* **2010**, *12*, 083038.
50. Nieskens, D. L. S.; van Bavel, A. P.; Niemantsverdriet, J. W. The Analysis of Temperature Programmed Desorption Experiments of Systems with Lateral Interactions; Implications of the Compensation Effect. *Surf. Sci.* **2003**, *546*, 159-169.
51. Stadtmüller, B.; Schröder, S.; Kumpf, C. Heteromolecular Metal–Organic Interfaces: Electronic and Structural Fingerprints of Chemical Bonding. *J. Electron Spectrosc. Rel. Phenom.* **2015**, *204*, 80-91.
52. Doniach, S.; Sunjic, M. Many-Electron Singularity in X-Ray Photoemission and X-Ray Line Spectra from Metals. *J. Phys. C: Solid State Phys.* **1970**, *3*, 285-291.
53. Topping, J. On the Mutual Potential Energy of a Plane Network of Doublets. *Proc. R. Soc. Lond. A* **1927**, *114*, 67-72.
54. Albano, E. V. A Model for the Work Function Change Caused by Coadsorption. *Appl. Surf. Sci.* **1983**, *14*, 183-193.
55. Witte, G.; Lukas, S.; Bagus, P. S.; Wöll, C. Vacuum Level Alignment at Organic/Metal Junctions: “Cushion” Effect and the Interface Dipole. *App. Phys. Lett.* **2005**, *87*, 263502.
56. Vázquez, H.; J. Dappe, Y. J.; Ortega, J.; Flores, F. Energy Level Alignment at Metal/Organic Semiconductor Interfaces: “Pillow” Effect, Induced Density of Interface States, and Charge Neutrality Level. *J. Chem. Phys.* **2007**, *126*, 144703.
57. Wellendorff, J.; Silbaugh, T. L.; Garcia-Pintos, D.; Nørskov, J. K.; Bligaard, T.; Studt, F.; Campbell, C. T. A Benchmark Database for Adsorption Bond Energies to Transition Metal Surfaces and Comparison to Selected Dft Functionals. *Surf. Sci.* **2015**, *640*, 36-44.
58. Maurer, R. J.; Liu, W.; Poltavsky, I.; Stecher, T.; Oberhofer, H.; Reuter, K.; Tkatchenko, A. Thermal and Electronic Fluctuations of Flexible Adsorbed Molecules: Azobenzene on Ag(111). *Phys. Rev. Lett.* **2016**, *116*, 146101.
59. Bader, R. F. W. *Atoms in Molecules - a Quantum Theory*. Oxford University Press: Oxford, **1990**.
60. Kruszewski, J.; Krygowski, T. M. Definition of Aromaticity Basing on the Harmonic Oscillator Model. *Tetrahedron Lett.* **1972**, *13*, 3839-3842.
61. Diederich, F.; Staab, H. A. Benzenoid Versus Annulenoid Aromaticity: Synthesis and Properties of Kekulene. *Angew. Chem. Int. Ed.* **1978**, *17*, 372-374.
62. Aihara, J.-i. Graph Theory of Aromatic Stabilization. *Bull. Chem. Soc. Jpn.* **2016**, *89*, 1425-1454.
63. Aihara, J.-i. Bond Resonance Energies of Polycyclic Benzenoid and Non-Benzenoid Hydrocarbons. *J. Chem. Soc. Perkin Trans. 2* **1996**, 2185-2195.
64. Jülich Supercomputing Centre, Jureca: Modular Supercomputer at Jülich Supercomputing Centre. *J. Large-scale Res. Fac.* **2018**, *4*, A132.

TOC GRAPHIC

